Modelling quasar outflows: clumpy winds and broad emission lines

J. H. Matthews[1,1], C. Knigge[1], N. Higginbottom[1], K. S. Long[2], S. A. Sim[3] and S. W. Mangham[1]

[1]School of Physics and Astronomy, University of Southampton, Highfield, Southampton, SO17 1BJ, United Kingdom
[2]Space Telescope Science Institute, 3700 San Martin Drive, Baltimore, MD, 21218
[3]School of Mathematics and Physics, Queens University Belfast, University Road, Belfast, BT7 1NN, Northern Ireland, UK

July 23, 2015

ABSTRACT

Various unification schemes for quasars and luminous active galactic nuclei (AGN) have proposed that the broad emission line region is roughly cospatial with broad absorption line (BAL) gas and much of the phenomenology of luminous AGN can be explained by a simple geometrical picture involving an accretion disc and associated outflow. Here, we test this paradigm by utilising our state-of-the-art radiative transfer code to produce synthetic spectra from simple biconical disc wind models. In particular, we expand on our previous work in which a benchmark model for BAL quasars was produced. We find that a simple treatment of clumping ('microclumping') allows for a more realistic X-ray luminosity in the model by lowering the ionization parameter. We examine the X-ray properties of this new model and find good agreement with existing X-ray samples of AGN and QSOs. We find that clumping enhances the H recombination and collisionally excited resonance lines, causing strong line emission (EW=?) to emerge at the low inclination angles, which represent quasars within this unification scenario. However, we are unable to produce line emission with comparable equivalent widths to existing quasar composites, due to a fundamental constraint arising from the anisotropy of emission from a classical thin disc. We briefly explore the effect of relativistic beaming, gravitational redshift and light bending on the angular distribution of disc continuum emission. We find that these general relativistic effects do cause the disc to emit more isotropically, but this is not yet sufficient to produce a self-consistent model. We discuss a number of potential solutions. Overall, our work suggests that geometric unification involving an accretion disc wind is a promising scenario, but our results pose a number of difficult challenges to such a model.

[1]jm8g08@soton.ac.uk

1. Introduction

The spectra of quasars and luminous active galactic nuclei (AGN) typically exhibit a series of strong emission lines with an underlying blue continuum - the so-called *'big blue bump'* (BBB). The BBB is normally attributed to emission from a geometrically thin, optically thick accretion disc surrounding the central black hole (REF), similar to that described by Shakura & Sunyaev (1973). In addition to the inflowing accreting material, outflows are ubiquitous in AGN and quasars (Kellermann et al. 1989; Ganguly & Brotherton 2008). These outflows can take the form of highly collimated radio jets (e.g. Hazard et al. 1963; Potash & Wardle 1980; Perley et al. 1984; Marscher 2006), or mass-loaded 'winds' emanating from the accretion disc (Weymann et al. 1991; Turner & Miller 2009). Outflows in AGN offer a potential feedback mechanism through which the central source can affect its environment (King 2003, 2005; Fabian 2012) – feedback that is required in models of galaxy evolution (REFs) and may explain the '$M-\sigma$' relation (Silk & Rees 1998; Häring & Rix 2004).

Approximately 20% of quasars exhibit broad absorption lines (BALs) in the ultraviolet, providing clear evidence for outflowing absorbing material (Weymann et al. 1991; Reichard et al. 2003; Knigge et al. 2008; Turner & Miller 2009; Allen et al. 2011). The simplest explanation for the incidence of BAL quasars (BALQSOs) is in terms of an accretion disc wind (ADW). Within this paradigm, the BALQSO fraction is associated with the covering factor of the outflow. In addition, ADWs may offer a natural explanation for the diverse phenemonology of luminous AGN and QSOs (e.g. Murray et al. 1995; Elvis 2000). In such a model, a biconical wind rises from the accretion disc, and the class of object is explained by the material intercepting the line of sight. Depending on viewing angle, an observer may then see a BALQSO or normal 'Type 1' quasar. Within this framework, the broad-line region (BLR) is normally assumed to correspond to the dense wind base. There are various spectroscopic sub-classifications of BALQSOs: HiBALQSOs, which only exhibit higher ionization line absorption; LoBALQSOs which also show absorption in lower ionization state species such as Mg II and Al III; and FeLoBALQSOs which show further absorption in Fe II and III. In unified models, this is generally attributed to ionization stratification of the outflow (e.g. Elvis 2000).

As well as imprinting clear line absorption features, disc wind may also have a profound effect on the structure and emergent *continuum* of the accretion disc itself. Mass-loss will alter the accretion rate and resultant temperature of the accretion disc, possibly explaining some of the features we typically see in luminous AGN (Laor & Davis 2014). Recent results from Capellupo et al. (2015) find that if one includes a combination of mass-loss, general relativity (GR) and Comptonisation then AGN spectral energy distributions (SEDs) can, in general, be fitted well with accretion disc models. Mass-loss therefore appears to be critical if an α-disc model is to successfully fit AGN SEDs, particular in the UV region of the spectrum.

Despite the clear importance of ADWs in understanding AGN SEDs and accretion physics, much of the underlying outflow physics remains highly uncertain. Several possible driving mecha-

nisms for ADWs have been proposed, including thermal pressure (Weymann et al. 1982; Begelman et al. 1991), magnetocentrifugal forces (Blandford & Payne 1982; Pelletier & Pudritz 1992) and radiation pressure on spectral lines ('line-driving'; Lucy & Solomon 1970; Shlosman et al. 1985; Murray et al. 1995). Of these, line-driving is possibly the most attractive, as strong absorption lines are already seen in BALQSOs and the X-ray spectra of AGN (Reeves et al. 2003; Pounds & Reeves 2009; Tombesi et al. 2010). The presence of line-locked features (Bowler et al. 2014) and the 'ghost of Ly α' (Arav et al. 1996; Arav 1996; North 2006; but see also Cottis et al. 2010) in the spectra of some BALQSOs also gives clearer evidence that line-driving is at least partially contributing to the acceleration of the wind.

The efficiency of line-driving is crucially dependent on the ionization state of the outflowing plasma. Murray et al. (1995) proposed a potential solution: a region of 'hitchhiking gas' that could shield the wind from the central X-ray source. Hydrodynamic simulations of line-driven disc winds also found a shielding region was required to maintain the correct ionization state (Proga et al. 2000; Proga & Kallman 2004). However, Higginbottom et al. (2014) showed that including multiple scattering means the ionizing radiation field could still reach the previously shielded regions in those particular models. An alternative solution is that the wind is clumped (e.g. Hamann et al. 2013) possibly on multiple scale lengths. Local density enhancements could lower the ionization parameter of the plasma while still maintaining the same mass-loss rate and column density.

Evidence for dense substructures in AGN winds is widespread. BALQSOs show complex absorption line profiles (Ganguly et al. 2006; Simon & Hamann 2010) and exhibit variability in these profile shapes (Capellupo et al. 2011, 2012, 2014). AGN generally show variability in X-ray absorption components (e.g. Risaliti et al. 2002) and many models for the BLR consist of clumps embedded in an outflow (Krolik et al. 1981; Emmering et al. 1992; de Kool & Begelman 1995; Cassidy & Raine 1996). Clumping can be caused by magnetic confinement de Kool & Begelman (1995), or the instabilities inherent to line-driven winds (Lucy & Solomon 1970; MacGregor et al. 1979; Carlberg 1980; Owocki & Rybicki 1984, 1985). Additionally, clumping is required in line-driven hot star winds in order to explain observations (Hillier 1991). Complex substructures on a variety of scales are also produced in simulations of line-driven outflows in AGN (Proga et al. 2000; Proga & Kallman 2004; Proga & Kurosawa 2010; Proga et al. 2014). Clumpy winds therefore offer an observationally motivated and theoretically predicted way to lower the ionization state of a plasma, possibly in tandem with a shielding scenario.

There has been some success using simple kinematic prescriptions for biconical disc winds to model AGN and quasar outflows (Sim et al. 2008; Higginbottom et al. 2013). (Higginbottom et al. 2013, hereafter H13), successfully produced a benchmark model for BALQSOs. However, the model had two key drawbacks. Firstly, an unrealistically low X-ray luminosity was required in order to prevent over-ionization of the outflow. Secondly, the model failed to produce the strong emission lines required at low inclinations in a unified model. In this paper, we attempt to address these issues, and test the disc wind unification model using Monte Carlo radiative transfer (MCRT) and photoionization calculations. The paper is organised as follows. In section 2, we describe our

code. In section 3, we outline the model, including a description of our clumping prescription. In section 4, we present the results from a clumped model. In section 5 we discuss our results, focussing particular on the anisotropy of disc emission and GR effects, and finally, in section 6, we summarise our findings.

2. Ionization and Radiative Transfer

We use the MCRT code PYTHON to carry out our radiative transfer and photoionization calculations in non-local thermodynamic equilibrium (non-LTE). The code is described extensively by a series of authors (LK02, S05, H13, M15). For that reason we only briefly describe the key elements of the global ionization calculation and other important aspects.

2.1. Line transfer

To treat line transfer, we adopt the same hybrid scheme described by M15, in which the energy flows through the system are described in terms of indivisible energy quanta of radiant or kinetic energy ('$r-$packets' and '$k-$packets' respectively; see also section 2.3). These energy packets interacting with either 'simple ions' or 'macro-atoms'. The macro-atom implementation is described in full by Lucy (2002, 2003). The scheme allows one to treat non-LTE line transfer in radiative equilibrium without approximation for elements which are identified as full macro-atoms, while maintaining the fast 'two-level' treatment of resonance lines when elements are identified as simple-ions. In this study, only H & He are treated as macro-atoms, because we expect recombination to be important in determining their level populations (see M15).

2.2. Ionization Scheme

Macro-atoms have their ion and level populations derived from MC rate estimators as described by M15. Previously (LK02, H13, M15), we adopted a modified Saha approach to calculate the ionization fractions of simple-ions. We have now improved our code to explicitly solve the rate equations in between ions in non-LTE. Not only does this dispense with a number of small assumptions made in the modified Saha approach, it is also more numerically stable, and in principle allows the direct addition of extra physical processes such as Auger ionization, which would have to be approximated if using the previous technique.

To avoid approximating the complex AGN SED as e.g. a dilute blackbody (Mazzali & Lucy 1993, M15), we model the SED in a cell using the technique described by H13. In this scheme, the mean intensity in a series of bands is modeled as a normalised power law in frequency ν

$$J_{\nu,j} = K_{pl}\nu^{\alpha_{pl}}, \tag{1}$$

for a band j, or an exponential

$$J_{\nu,j} = K_{exp} e^{(-h\nu/kT_{exp})}. \tag{2}$$

Here, K_{exp}, K_{pl}, T_{exp} and α_{pl} are spectral fit parameters deduced from the band-limited radiation field estimators. The ionization rate out of ion i can then be written as

$$R_{i,i+1}(J) = n_i \left(C_i n_e + \sum_{band\ j=0}^{n} \int_{\nu_j}^{\nu_j+1} J_{\nu,j} \sigma_i(\nu) \nu^{-1} d\nu \right), \tag{3}$$

where σ_i is the photoionization cross-section and C_i represents the collisional ionization coefficient. The recombination rate *into* ion i is simply given by

$$R_{i+1,i}(T_e) = (\alpha^i_{RR} + \alpha^i_{DR} + \alpha^i_{CR}) n_{i+1} n_e \tag{4}$$

Where each α here is the recombination rate coefficient into the ground state of ion i. The subscripts denote radiative, dielectronic and collisional (three-body) recombination respectively. We thus neglect recombination to and from excited states in the simple-ion calculation. For simple-ions, we use a dilute Boltzmann equation to calculate the population of level k in ionic stage j,

$$\frac{n_{jk}}{n_j} = \frac{W g_k}{z_j(T_R)} \exp(-E_k/kT_R). \tag{5}$$

Here z_j is the partition function of ionic stage j, T_R is the effective radiation temperature, E_k is the energy difference between level k and the ground state, and g_k is the statistical weight of level k.

2.3. Physical Processes

We include all free-free, bound-free and bound-bound heating and cooling processes in the model. For radiative transfer purposes we treat electron scattering in the Thomson limit, but take full account of Compton heating and cooling when calculating the thermal balance of the plasma (see H13). Adiabatic cooling is included and represents the only departure from strict radiative equilibrium, but is insignificant in most of the outflow. It is dealt with self consistently by the spontaneous destruction of k-packets with a probability

$$P_{\text{adiabatic destruction}} = \frac{C_{\text{adiabatic}}}{C_{\text{total}}}, \tag{6}$$

where $C_{\text{adiabatic}}$ and C_{total} represent the adiabatic and total cooling rates in the cell.

2.4. Atomic Data

We use the same atomic data as described by LK02 and since updated by H13 and M15, with the addition of direct ionization data from Dere (2007). Photoionization cross-sections are from

TOPBASE (Cunto et al. 1993) and Verner et al. (1996). Dielectronic and radiative recombination rate coefficients are taken from the CHIANTI database version 7.0 (Dere et al. 1997; Landi et al. 2012). We use ground state recombination rates from Badnell (2006) where available, and otherwise default to calculating recombination rates from the Milne relation. Free-free Gaunt factors are from Sutherland (1998).

3. A Clumpy Biconical Disk Wind Model for Quasars

Our kinematic prescription for a biconical disc wind model follows Shlosman & Vitello (1993), and is described further by LK02, H13 and M15. A schematic is shown in figure 1, with key aspects marked. The general biconical geometry is similar to that invoked by Murray et al. (1995) and Elvis (2000) in order to explain the phenomenonology of quasars and BALQSOs.

3.1. Photon Sources

The accretion disc in our model is geometrically thin, but optically thick and this adopt a standard multi-temperature blackbody using a Shakura & Sunyaev (1973) temperature profile. The emergent SED is thus determined by the specified accretion rate ($\dot{m}$) and central BH mass (M_{BH}). The inner radius of the disc extends to the innermost stable circular orbit (ISCO) of the BH. We assume a Schwarzchild BH with an ISCO at 6 R_G. The X-ray source in our model is treated as an isotropic sphere at the ISCO, which emits photons according to a power law with index α_X. The normalisation of this power law is such that it produces the specified 2-10kev luminosity. In addition to the disc and X-ray source, the wind is able to reprocess radiation. However, new photon packets are not produced in the wind (as in LK02). Instead, this reprocessing is dealt with by enforcing strict radiative equilibrium via an indivisible energy packet constraint (see Lucy 2002, M15).

3.2. Kinematics and Geometry

Describe briefly the kinematics and geometry of the model.

3.3. Clumping

To take account of clumping in our outflow we adopt a simple parameterization used in stellar wind modelling, known as *microclumping* (Hamann & Koesterke 1998). The key assumption here is that typical clump sizes are much smaller than the typical photon mean free path, and thus the clumps are both geometrically and optically thin. This approach is typically known as micro-

clumping and allows one to introduce a 'filling factor', f, which is the fraction of the volume of the plasma filled by clumps. We can then introduce the density enhancement, D, which is simply defined as

$$D = \frac{1}{f}. \tag{7}$$

We then multiply all densities in the model by D, and all emitting volumes by f, meaning that all ρ^2 emissivities and opacities (such as collisional excitation and recombination) will be enhanced, while all ρ process (such as electron scattering and bound-free opacity) remain unchanged for a given ionization state.

Clumping the wind has an important effect on the ionization state and has been proposed as a solution to the so-called 'over-ionization problem' in disc winds (REFs). This is the main motivation for incorporating microclumping into our model. This treatment is first-order; it does not adequately represent the complex substructures and stratifications in ionization state we expect in AGN outflows. Nevertheless, clumping is clearly important in these flows, and this parameterization allows a simple estimate for the effect clumping might have on the ionization state and emergent line emission. It is also encouraging that microclumping has been used successfully in fits to O-star wind spectra (REFs).

4. Results

Here we describe the results from our model. This set of parameters was arrived at by conducting a limited grid search over a 5-dimensional parameter space involving the variables r_{min}, θ_{min}, f, α and R_V. We then evaluated these models qualitavely based on the following criteria:

- Does the model maintain the correct ionization state and produce strong BALs?
- Does strong line emission emerge at low inclinations?
- Do H recombination lines appear in the spectrum?
- Do a certain range of angles produce LoBAL features?

We arrived at a model which is one of the most promising, but also representative of a family of models. Examination of this individual model allows us to gain insight into fundamental geometrical and physical constraints, as discussed in section 5. The full grid, including output spectral files and plots can be found at `jhmatthews.github.io/quasar-wind-grid/`.

4.1. Physical Conditions and Ionization State

The wind rises slowly from the disc at first, with clumped densities of $n_H \sim 10^{11}$ cm^{-3} close to the disc plane. The flow then accelerates over a scale length of $R_V = 10^{19}$ cm up to a terminal

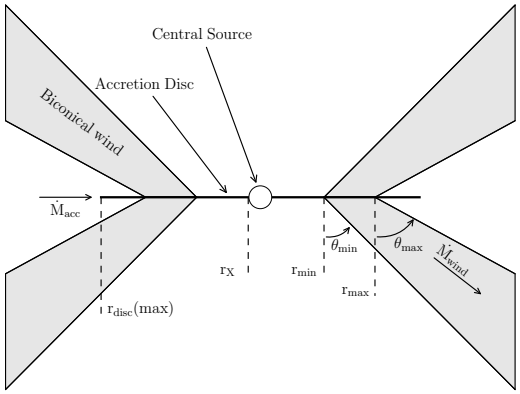

Fig. 1.— A cartoon showing the geometry and some key parameters of our biconical wind model.

Free Parameters	Value
M_{BH}	1×10^9 M$_\odot$
$\dot{M}_{acc}$	5 $M_\odot yr^{-1} \simeq 0.2$ $\dot{M}_{Edd}$
α_X	-0.9
L_X	10^{45} ergs s^{-1}
$r_{disc}(min) = r_X$	$6r_g = 8.8 \times 10^{14}$ cm
$r_{disc}(max)$	$3400r_g = 5 \times 10^{17}$ cm
$\dot{M}_{wind}$	5 $M_\odot yr^{-1}$
r_{min}	$300r_g = 4.4 \times 10^{16}$ cm
r_{max}	$600r_g = 8.8 \times 10^{16}$ cm
θ_{min}	70.0°
θ_{max}	82.0°
λ	0
v_∞	v_{esc}(f=1)
R_v	10^{19}cm
α	1.0
f	0.01

Table 1: Wind geometry parameters used in the model.

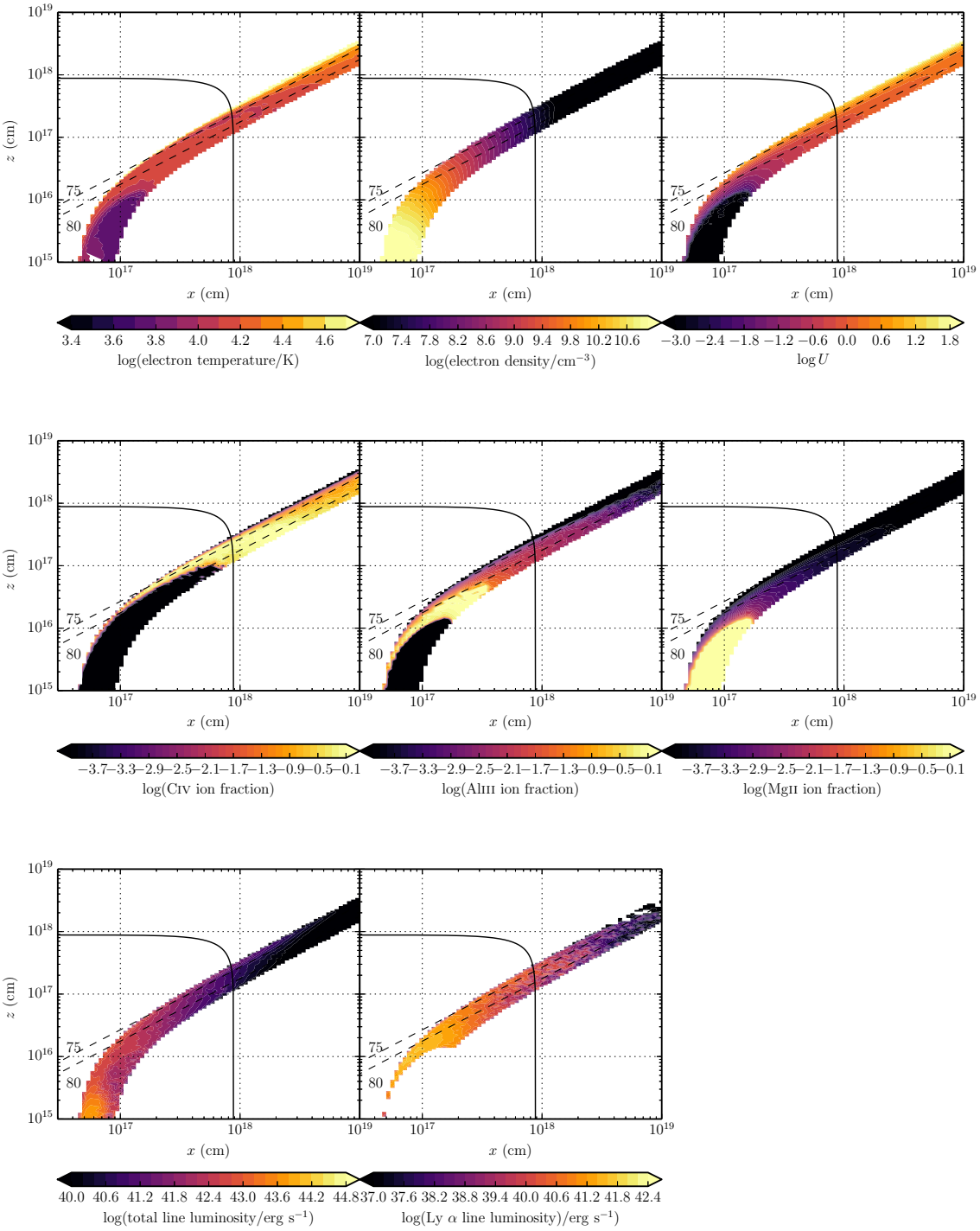

Fig. 2.— Physical properties of the outflow, shown by the coloured contours. The solid black line marks a sphere at 1000 R_G. The dotted lines show the 75° and 80° sightlines to the centre of the system, and illustrate that different sightlines intersect material of different ionization states.

velocity of around 3 times the escape velocity ($\sim 10,000$ km s^{-1}). This gradual acceleration means that the wind exhibits a stratified ionization structure, with low ionization material in the base of the wind giving way to highly ionized plasma further out. By clumping the wind, we are able to produce the range of ionization states observed in Quasars and BALQSOs, while adopting a realistic $2-10$ keV X-ray luminosity of $L_X = 10^{45}$ ergs s^{-1}. Without clumping, this wind would be over-ionized to the extent that opacities in e.g., C IV would be entirely negligible (see H13).

One commonly used measure of the ionization state is the ionization parameter, U, given by

$$U = \frac{4\pi}{n_H c} \int_{13.6\mathrm{eV}}^{\infty} \frac{J_\nu d\nu}{h\nu}. \tag{8}$$

where n_H is the local number density of H, and ν denotes photon frequency. The ionization parameter represents the ratio of the number density of ionizing photons to the local H density. It is however, a poor measure of the ionization state of the resonance species such as C IV as it encodes no information about the shape of the SED. In this case the X-ray photons are dominant in the photoionization of the UV resonance line ions. This explains why a factor of 100 increase in X-ray luminosity requires a clumping factor of 0.01, even though the value of U changes by roughly ?? compared to H13.

Clumping also causes the total line luminosity to increase dramatically, as recombination and collisional excitation are both proportional to n_e^2. This line emission typically emerges on the edge of the wind nearest the central source. The location of the line emitting regions is dependent on the ionization state, as well as the X-rays heating the plasma. The radii of these emitting regions is important, and can be compared to observations. Our C IV line emission region is located at about 1000 R_G ($\sim 10^{18}$ cm). This is in rough agreement with the reverberation mapping results of Kaspi (2000) for the $2.6 \times 10^9 M_\odot$ quasar S5 0836+71, and also compares favourably with microlensing measurements of the size of the C IV emission line region in the BALQSO H1413+117 (O'Dowd et al. 2015).

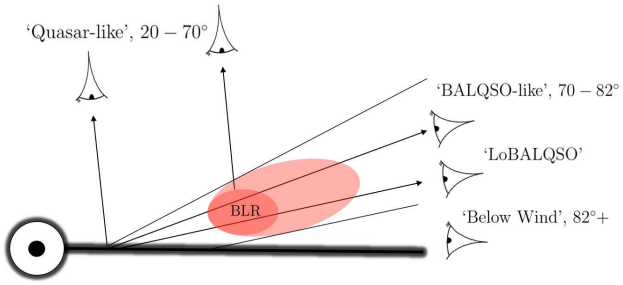

Fig. 3.— The classes of sightlines and the corresponding possible system types in the framework of our model.

4.2. Synthetic Spectra

Figure 4 shows the synthetic spectrum in the UV from the two models, with the benchmark model from H13 also shown for comparison. We also show a comparison to composite quasar and BALQSO spectra in figure 5, with the optical waveband included. In the UV, strong BAL profiles are formed in both models. This highlights the first success of our model: clumping allows the correct ionization state to be maintained in the presence of strong X-rays. The BAL profiles are saturated, and generally show the strongest absorption at the terminal velocity. This contradicts observed profiles of many BALQSOs (REFs), although there are some objects which do show this behaviour (REFs). However, we have found that this profile shape is by no means ubiquitous. Figure 6 shows how the line profile varies with angle for three of the UV lines (see also section 4.4). In addition, the line profile shape is strongly dependent on the density, ionization and velocity profiles intersected by the line of sight. Thus, small tweaks of the velocity law and angular distributions of streamlines can dramatically alter the line profile shape. Figure ?? shows selection of line profiles for different kinematic parameters to demonstrate this. The degeneracy between parameters, and lack of available physical and observational constraints goes someway to showing why individual fitting of line profile shapes with kinematic models is such a difficult exercise.

We find that model A can produce significant line emission at low inclinations, particular in C IV, and the improved treatment of recombination results in a strong Ly α line. However, the red wing of the BAL profiles is far stronger than seen in BALQSO spectra and composites. This is due to a combination of strong collisionally excited emission and continuum attenuation. To illustrate the amount of continuum attenuation we also show the continuum from a disc-only model. The line-to-continuum ratios at low inclinations are also significantly affected by disc foreshortening and limb darkening. The angular distribution of the disc radiation is clearly crucially important in determining the emergent line equivalent widths (EWs) – this is discussed further in section 5.

To assess the ability of the model to match real quasar spectra, we show a comparison to an HST quasar composite in figure 5. All the spectra are normalised to the flux at 2000Åin these plots. Model A matches the C IV line profile well, but the Ly α profile is a factor of ~ 3 weaker than in the composite spectrum. Figure 5 also shows the spectrum into the optical, showing that the outflow produces signiciant optical emission lines as well as having a noticeable effect on the continuum shape. This is particularly true around the Balmer jump at $3646\mathring{A}$ and is due to a prominent wind-formed recombination continuum.

4.3. X-ray Properties and Broadband SEDs

The bottom panel of figure 7 shows the emergent L_{2keV} monochromatic luminosity (L_ν) and α_{OX} plotted against L_ν at 2500Å for a number of different viewing angles in our model. α_{OX} is a spectral index from near UV to X-rays defined by

$$\alpha_{OX} = 0.3838 \log \left(\frac{L_\nu(2\ keV)}{L_\nu(2500\ \text{Å})} \right). \quad (9)$$

The properties are calculated from the synthetic spectra and thus include the effects of wind reprocessing and attenuation. In addition to model outputs, we also show the BALQSO sample of Saez et al. (2012) and luminous AGN and quasar samples from Steffen et al. (2006). For low inclination, 'quasar-like' viewing angles, we now show excellent agreement with AGN samples. The trend with inclination in our models is caused by a combination of disc foreshortening/limb-darkening (resulting in a lower L_{2500} for higher inclinations) and the fact that the disk is opaque and thus the X-ray source subtends a smaller solid angle at high inclinations (resulting in a lower L_{2keV} for higher inclinations).

Although the low inclination, 'BALQSO-like' viewing angles show moderate agreement with the data, it appears that our models tend to underpredict the emergent X-ray luminosity at although we are limited by poor statistics. It is possible that this is due to our wind being overly optically thick to electron scattering at angles which look through the wind. It could also be that the isotropic X-ray source assumption is incorrect and BALQSOs are *intrinsically* X-ray weak (e.g. Morabito et al. 2013). Nevertheless, our input X-ray spectrum now reproduces the X-ray properties of a luminous quasar.

Typically, BALQSOs show strong X-ray absorption with columns of $N_H \sim 10^{23}$ cm^{-2} (Green & Mathur 1996; Brandt et al. 2000; Mathur et al. 2000; Green et al. 2001; Grupe et al. 2003). This is often cited as evidence that the BAL outflow is shielded from the X-ray source, especially as sources with strong X-ray absorption tend to exhibit deep BAL troughs and high outflow velocities (REFs). Our results tend to imply that a clumpy BAL outflow itself can be responsible for the strong X-ray absorption, and possibly explains why mini-BALs have weaker X-ray absorption than BALQSOs (e.g. Brandt et al. 2000; Hamann et al. 2013).

We can also examine the emergent X-ray spectra from our model. Our code is not yet optimized for producing X-ray spectra, as we do not yet include all lines and levels of e.g. Fe or macro-atom treatments of higher order ions (cf. Sim et al. 2008, 2010). However, the bound-free opacity sources are complete, and comparisons of the shape of the heavily absorbed spectra can be useful. Figure 6 shows the broadband SED from the model, compared to a number of BALQSO spectra from Grupe & Nousek (2015) - note that lower mass and super-Eddington sources are excluded.

4.4. LoBALs and ionization stratification

At certain sightlines, our model now produces blue-shifted BALs in Al III and Mg II– the absorption lines seen in LoBALQSOs. Line profiles in velocity space for C IV, Al III and Mg II, are shown in figure 8 for a range of BALQSO viewing angles. We confirm the behaviour expected from a unification model such as Elvis (2000), in which ionization stratification explains the incidence of

LoBALQSOs. In this framework, the lower ionization material is intercepted by a smaller family of sightlines. This is also the explanation here, as shown by figure **??**.

These line profiles also indicate a potential problem with our model. O'Dowd et al. (2015) find that the LoBAL profiles in H1413+117 have a higher velocity onset than the higher ionization BALs, suggesting that the wind becomes less ionized as radius increases. We find the opposite trend in velocity onsets. In addition, examination of figure **??** shows that ionization parameter decreases with radius, because the decrease in density wins over geometric dilution of the radiation field. While the O'Dowd et al. (2015) hypothesis comes from one object, it is clear that *at least some* BALQSOs must become less ionized at higher velocities, contrary to what one expects from our modelling.

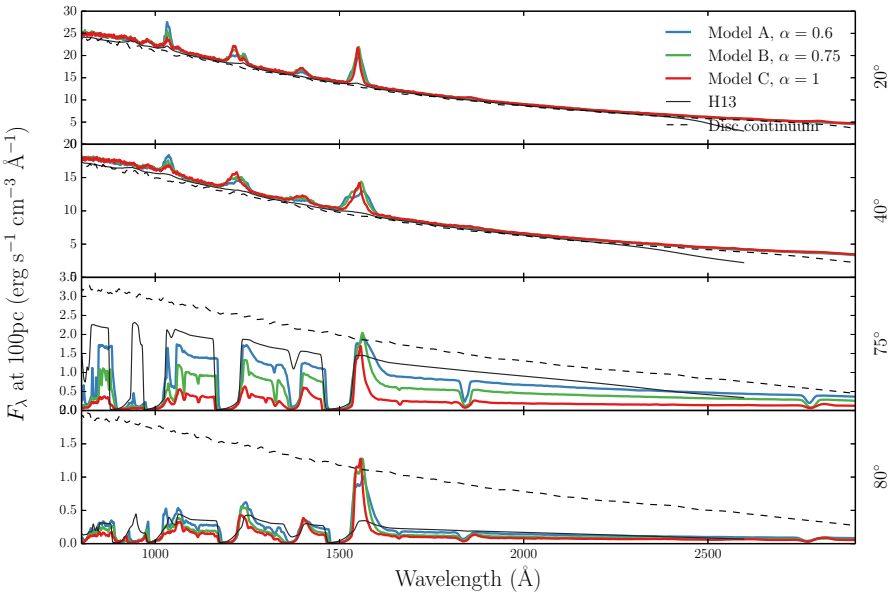

Fig. 4.— Synthetic spectra at four viewing angles in the clumpy model. Plot would look different probably, and may show composites, but this would be the main synthetic spectrum plot.

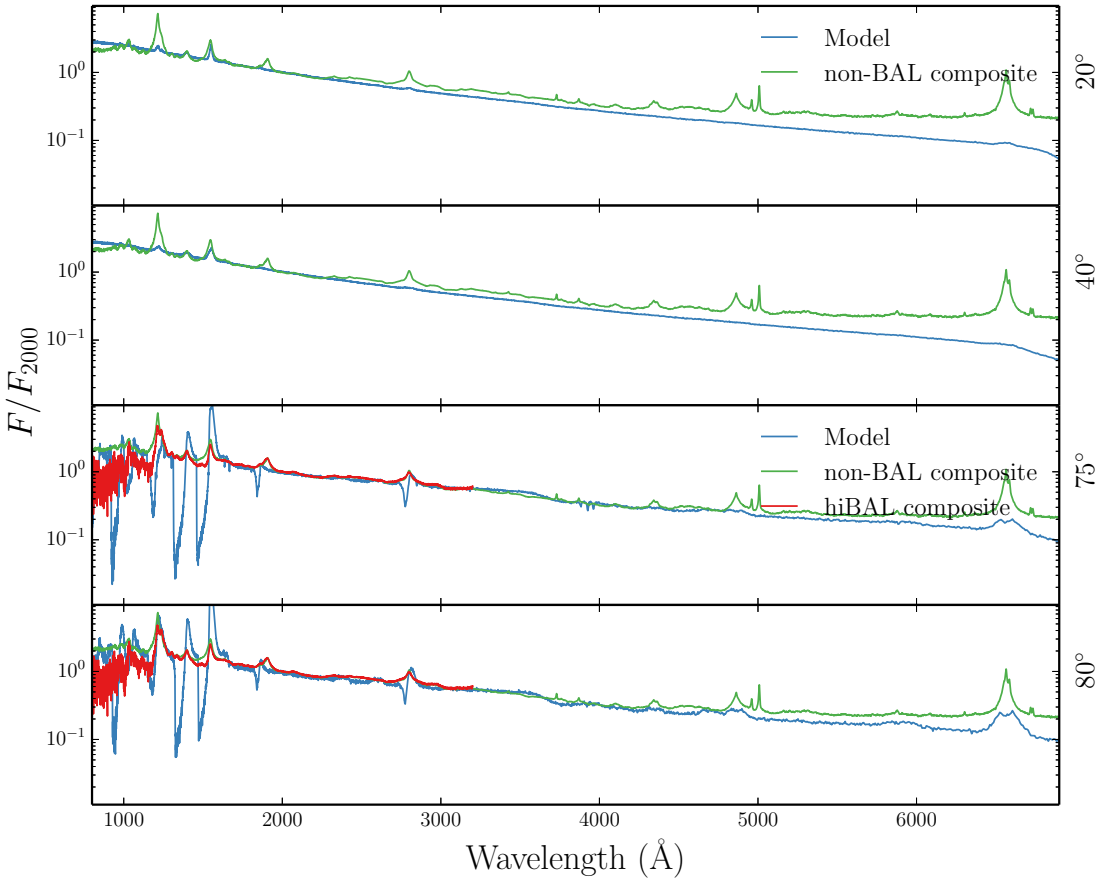

Fig. 5.— Figure designed to show optical spectrum and comparison to composite.

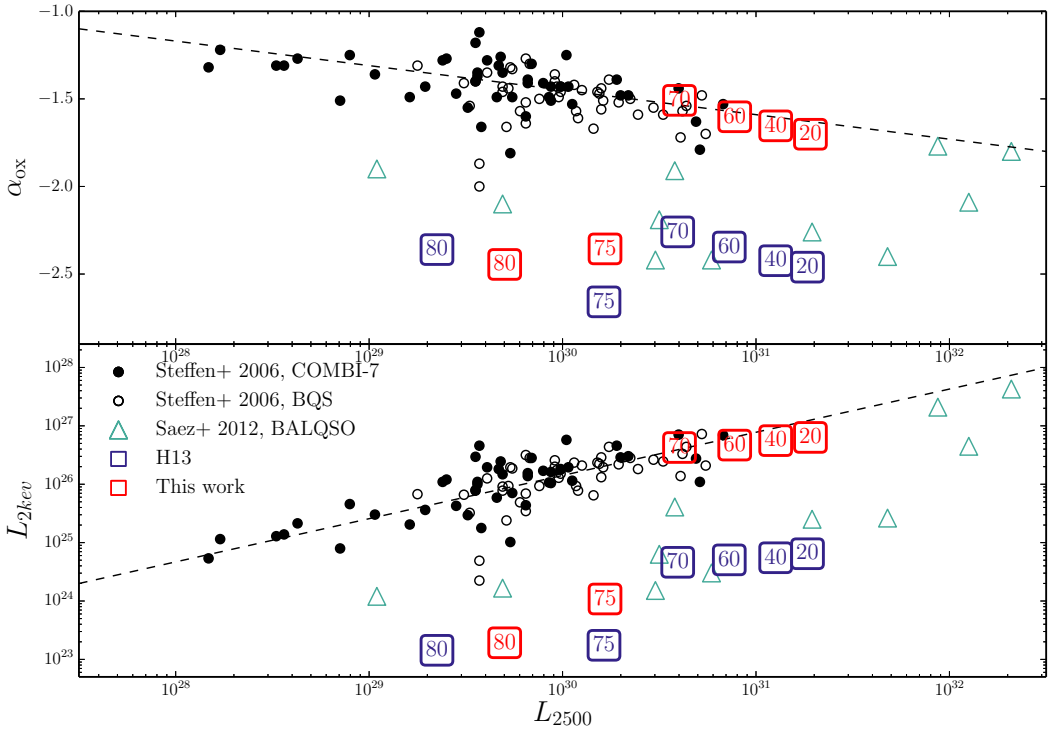

Fig. 6.— X-ray properties of the H13 and clumped model (text filled squares), plotted against monochromatic luminosity at 2500Å. Also plotted are the samples considered by Saez et al. 2012 on a similar plot; The COMBI-7 AGN sample (ref), the BQS sample (ref) and the Saez et al. (2012) sample of BALQSOs.

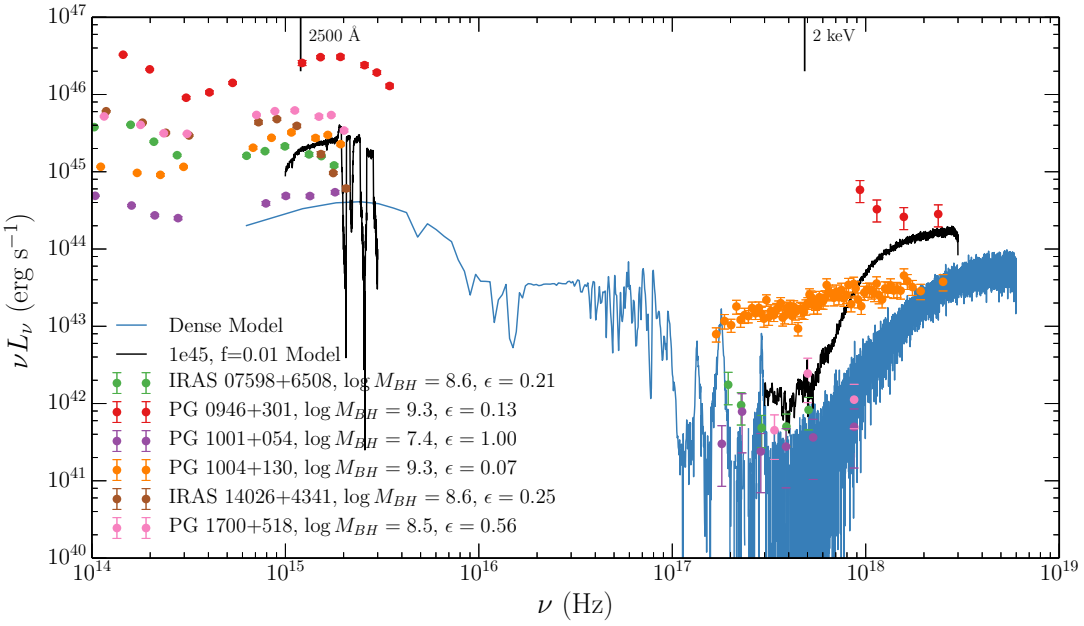

Fig. 7.— Broadband SEDs compared to IR and X-ray SEDs for selected BALQSOs from Grupe & Nousek (2015).

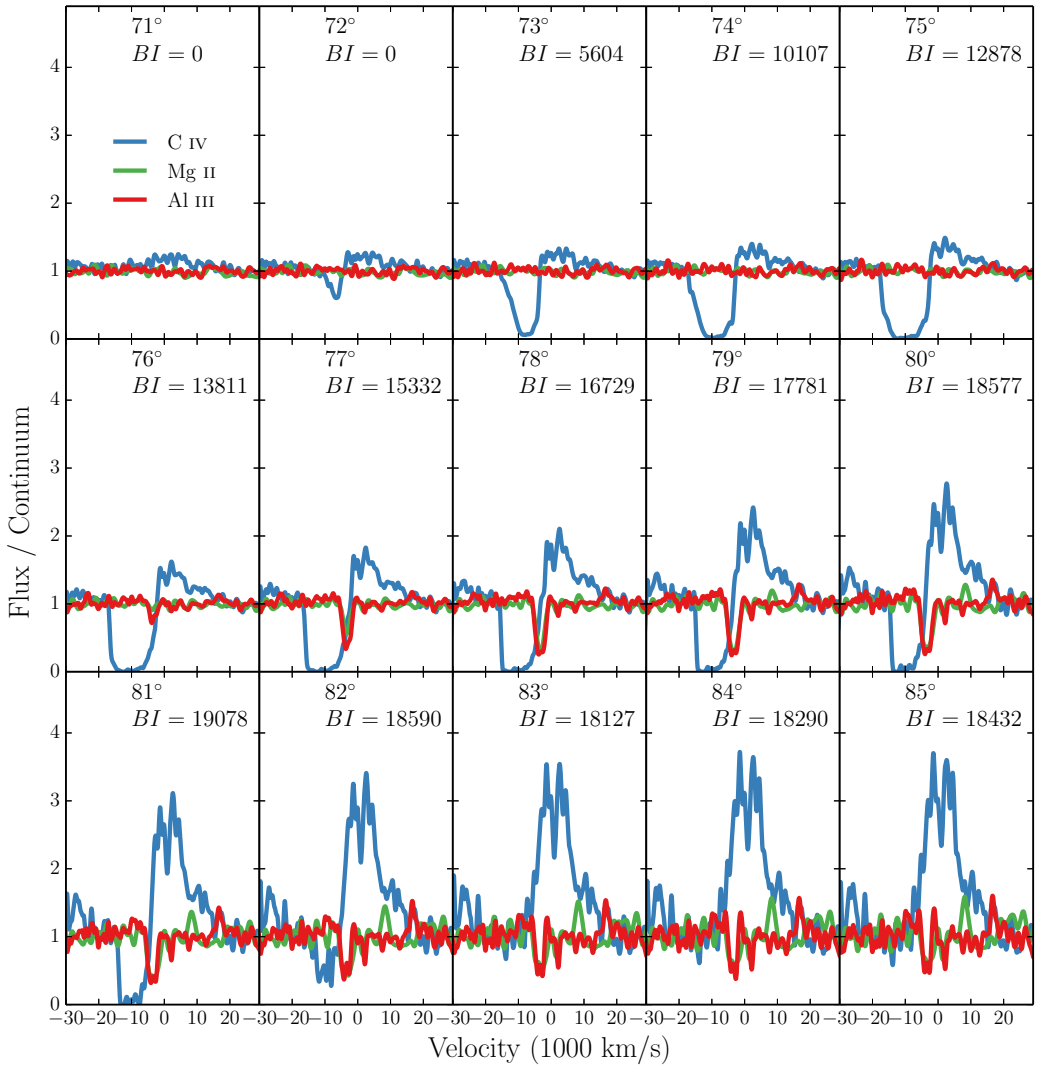

Fig. 8.— Carbon IV, Al III and Mg II line profiles with inclination for wind angles. Showing how the line profiles change and how LoBALs kick in at particularly high inclinations.

5. Discussion: The Disc SED

5.1. Anisotropy of disc emission

Discuss the importance of the angular distribution of the disc SED on line (limb-darkened, foreshortened, etc.)

5.2. General relativistic effects

General relativistic effects – specifically, light bending and relativistic beaming – can cause the accretion disc SED to become more isotropic (e.g. Zhang et al. 1997; Muñoz-Darias et al. 2013). To generate GR disc spectra, we use the code AGNSPEC (Hubeny et al. 2000; Davis & Hubeny 2006; Davis et al. 2007). The output flux at 2000 Å as a function of inclination for an AGNSPEC model with the same disc and BH parameters as our clumpy wind model is shown in figure **??**. The effect of relativistic effects on disc anisotropy can be clearly seen.

To examine the effect of GR on our models, we carry out the following procedure. First, we fit our output spectrum with a polynomial. This continuum fit can be subtracted from the actual spectrum to produce a model of the line emission only. We then calculate the 'wind continuum factor', by comparing the model fit with the emergent disc spectrum without a wind. This factor gives us an approximate way to quantify the effect of the wind on a disc continuum. It will generally be > 1 at high inclinations, and < 1 at low inclinations. This calculates emergent accretion disc spectra from an AGN disc atmosphere including relativistic effects. Finally, produce our final synthetic spectrum by convolving this the line emission spectrum with the AGNSPEC model for the model parameters.

Figure 10 shows the resultant spectrum. Including GR clearly helps

5.3. Wind reprocessing

How would wind reprocessing help?

5.4. The BALQSO fraction and wind covering factor

The disc SED has a profound effect on the intrinsic BAL fraction inferred from flux-limited samples. This in turn impacts on the geometry and covering factor assumed for BALQSO and unified wind models, and even effects the efficiency of feedback. Krolik & Voit (1998) noted that the effect of limb darkening and foreshortening would result in a signicantly underestimated covering factor for BALQSO winds. The effect is complicated further by the quasar luminosity function –

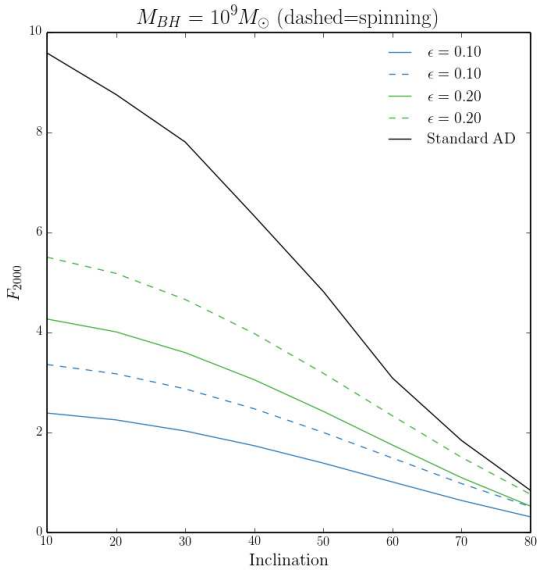

Fig. 9.— F_{2000} as a function of inclination from AGNSPEC models, compared to a classical AD. **This is a placeholder- it will show the effect of GR on the anisotropy of the disk for different wavelengths and eddington fractions, compared to limb darkened and foreshortened classical AD**.

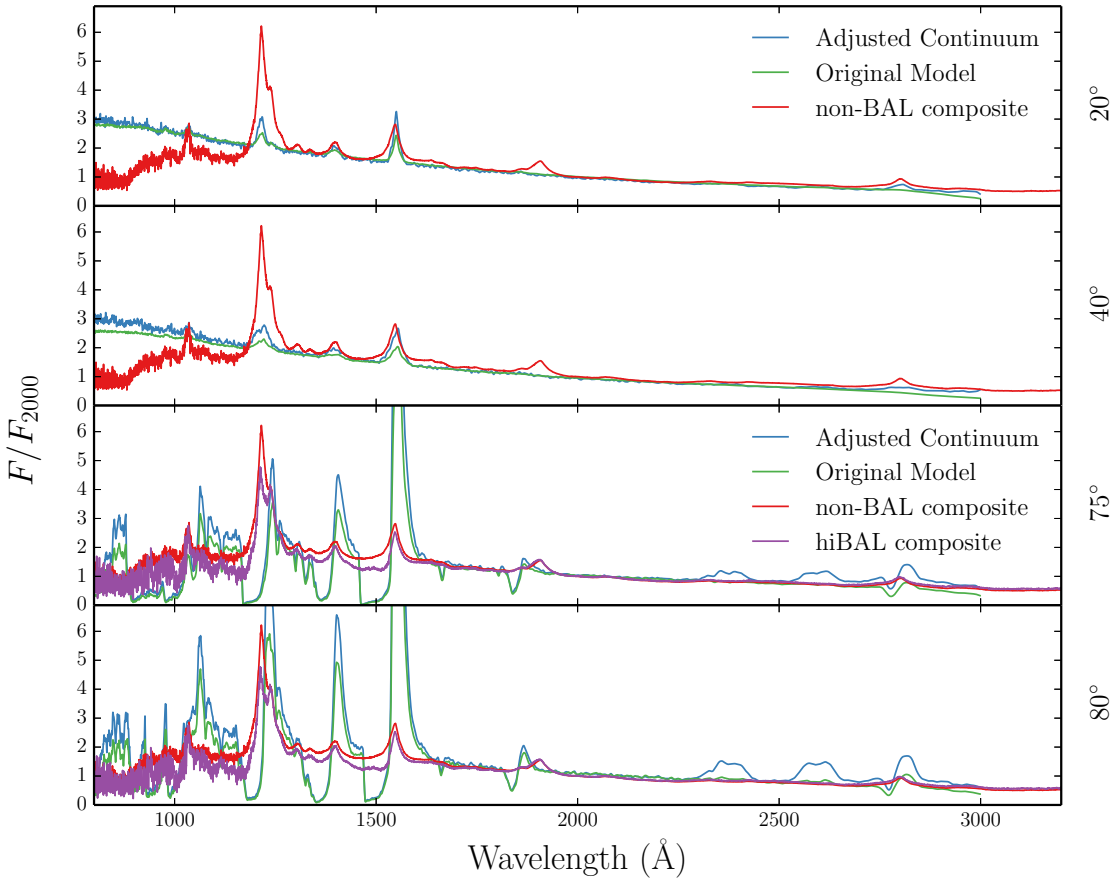

Fig. 10.— F_λ normalised to F_{2000}. **Again, this is a placeholder- but I'm thinking some kind of comparison to composite including the adjusted continuum, showing that we can't get it exactly right**.

if BALQSOs have lower observed luminosities for given accretion disc properties then they may be drawn from a different bin in the quasar luminosity function (Goodrich 1997). These effects are understandably not taken into account by current estimates of the intrinsic BALQSO fraction (Weymann et al. 1991; Reichard et al. 2003; Knigge et al. 2008; Turner & Miller 2009; Allen et al. 2011). The way forward is somewhat unclear. Given the lack of available observational constraints, models cannot readily be used to inform the selection criteria when calculating the BALQSO fraction. Nevertheless, understanding the true nature of the disc SED, including the angular distribution of radiation, is clearly crucial in order to accurately estimate the true covering factor of BALQSO winds.

6. Summary

We have carried out MCRT simulations using a simple prescription for a biconical disc wind, with the aim of expanding on the work of H13 and assessing the viability of such a model for geometric unification of quasars. We find the following main points:

1. We have introduced a first-order treatment of clumping in our model, and found that it can now maintain the required ionization state while agreeing well with the X-ray properties of AGN/QSOs.

2. We have shown that the degree of ionization stratification in the model is sufficient that LoBAL line profiles are seen at a subset of viewing angles.

3. We find that clumping also causes a significant increase in the strength of the emission lines produced by the model. This is true both of collisionally excited resonance lines (such as C IV, N V) and recombination lines (such as Ly α, H α and the Balmer series).

4. The line EWs in our models are not comparable to those in Quasar composite spectra. This is due to a fundamental constraint discussed in section ?. If the BLR emits fairly isotropically then for a foreshortened, limb-darkened classical thin accretion disc it is not possible to achieve line ratios at low inclinations that are comparable to those at high inclinations. This is a robust conclusion which is independent of the assumed BLR geometry.

5. We have examined the effect of GR on our disc SED, using the disc atmosphere and GR ray-tracing code AGNSPEC. While including GR effects does cause the disc SED to become significantly more isotropic, the effect is not large enough to produce uniform line to continuum ratios with viewing angle. We discuss other solutions to this problem in section ?; It is possible that a combination of GR and reprocessing by the wind could provide a solution, and a number of complicated selection effects may be at work in the building of the quasar composites.

Our work confirms a number of expected outcomes from such a model, and suggests that a simple geometry such as this can come close to explaining much of the phenomenology of quasars. Nevertheless, our conclusions pose a clear challenge to the current unification picture.

Acknowledgements

We would like to thank Omer Blaes, Ivan Hubeny, Shane Davis, Michael Crenshaw, Nahum Arav, Daniel Proga, Daniel Capellupo, Dirk Grupe etc.

REFERENCES

Allen J. T., Hewett P. C., Maddox N., Richards G. T., Belokurov V., 2011, MNRAS 410, 860

Arav N., 1996, ApJ 465, 617

Arav N., Korista K. T., Barlow T. A., Begelman, 1995, Nature 376, 576

Badnell N. R., 2006, ApJs 167, 334

Begelman M., de Kool M., Sikora M., 1991, ApJ 382, 416

Blandford R. D., Payne D. G., 1982, MNRAS 199, 883

Bowler R. A. A., Hewett P. C., Allen J. T., Ferland G. J., 2014, MNRAS 445, 359

Brandt W. N., Laor A., Wills B. J., 2000, ApJ 528, 637

Capellupo D. M., Hamann F., Barlow T. A., 2014, MNRAS 444, 1893

Capellupo D. M., Hamann F., Shields J. C., Rodríguez Hidalgo P., Barlow T. A., 2011, MNRAS 413, 908

Capellupo D. M., Hamann F., Shields J. C., Rodríguez Hidalgo P., Barlow T. A., 2012, MNRAS 422, 3249

Capellupo D. M., Netzer H., Lira P., Trakhtenbrot B., Mejía-Restrepo J., 2015, MNRAS 446, 3427

Carlberg R. G., 1980, ApJ 241, 1131

Cassidy I., Raine D. J., 1996, A&A 310, 49

Cottis C. E., Goad M. R., Knigge C., Scaringi S., 2010, MNRAS 406, 2094

Cunto W., Mendoza C., Ochsenbein F., Zeippen C. J., 1993, A&A 275, L5

Davis S. W., Hubeny I., 2006, ApJs 164, 530

Davis S. W., Woo J.-H., Blaes O. M., 2007, ApJ 668, 682

de Kool M., Begelman M. C., 1995, ApJ 455, 448

Dere K. P., 2007, A&A 466, 771

Dere K. P., Landi E., Mason H. E., Monsignori Fossi B. C., Young P. R., 1997, A&As 125, 149

Elvis M., 2000, ApJ 545, 63

Emmering R. T., Blandford R. D., Shlosman I., 1992, ApJ 385, 460

Fabian A. C., 2012, ARAA 50, 455

Ganguly R., Brotherton M. S., 2008, ApJ 672, 102

Ganguly R., Sembach K. R., Tripp T. M., Savage B. D., Wakker B. P., 2006, ApJ 645, 868

Goodrich R. W., 1997, ApJ 474, 606

Green P. J., Aldcroft T. L., Mathur S., Wilkes B. J., Elvis M., 2001, ApJ 558, 109

Green P. J., Mathur S., 1996, ApJ 462, 637

Grupe D., Mathur S., Elvis M., 2003, AJ 126, 1159

Grupe D., Nousek J. A., 2015, AJ 149, 85

Hamann F., Chartas G., McGraw S., Rodriguez Hidalgo P., Shields J., Capellupo D., Charlton J., Eracleous M., 2013, MNRAS 435, 133

Hamann W.-R., Koesterke L., 1998, A&A 335, 1003

Häring N., Rix H.-W., 2004, ApJ Letters 604, L89

Hazard C., Mackey M. B., Shimmins A. J., 1963, Nature 197, 1037

Higginbottom N., Knigge C., Long K. S., Sim S. A., Matthews J. H., 2013, MNRAS 436, 1390

Higginbottom N., Proga D., Knigge C., Long K. S., Matthews J. H., Sim S. A., 2014, ApJ 789, 19

Hillier D. J., 1991, A&A 247, 455

Hubeny I., Agol E., Blaes O., Krolik J. H., 2000, ApJ 533, 710

Kellermann K. I., Sramek R., Schmidt M., Shaffer D. B., Green R., 1989, AJ 98, 1195

King A., 2003, ApJ Letters 596, L27

King A., 2005, ApJ Letters 635, L121

Knigge C., Scaringi S., Goad M. R., Cottis C. E., 2008, MNRAS 386, 1426

Krolik J. H., McKee C. F., Tarter C. B., 1981, ApJ 249, 422

Krolik J. H., Voit G. M., 1998, ApJ Letters 497, L5

Landi E., Del Zanna G., Young P. R., Dere K. P., Mason H. E., 2012, ApJ 744, 99

Laor A., Davis S. W., 2014, MNRAS 438, 3024

Lucy L. B., 2002, A&A 384, 725

Lucy L. B., 2003, A&A 403, 261

Lucy L. B., Solomon P. M., 1970, ApJ 159, 879

MacGregor K. B., Hartmann L., Raymond J. C., 1979, ApJ 231, 514

Marscher A. P., 2006, in P. A. Hughes, J. N. Bregman (eds.), Relativistic Jets: The Common Physics of AGN, Microquasars, and Gamma-Ray Bursts, Vol. 856 of *American Institute of Physics Conference Series*, p. 1

Mathur S., Green P. J., Arav N., Brotherton M., Crenshaw M., deKool M., Elvis M., Goodrich R. W., Hamann F., Hines D. C., Kashyap V., Korista K., Peterson B. M., Shields J. C., Shlosman I., van Breugel W., Voit M., 2000, ApJ Letters 533, L79

Mazzali P. A., Lucy L. B., 1993, A&A 279, 447

Morabito L. K., Dai X., Leighly K. M., Sivakoff G. R., Shankar F., 2013, ArXiv e-prints

Muñoz-Darias T., Coriat M., Plant D. S., Ponti G., Fender R. P., Dunn R. J. H., 2013, MNRAS 432, 1330

Murray N., Chiang J., Grossman S. A., Voit G. M., 1995, ApJ 451, 498

North M., Knigge C., Goad M., 2006, MNRAS 365, 1057

O'Dowd M. J., Bate N. F., Webster R. L., Labrie K., Rogers J., 2015, ArXiv e-prints

Owocki S. P., Rybicki G. B., 1984, ApJ 284, 337

Owocki S. P., Rybicki G. B., 1985, ApJ 299, 265

Pelletier G., Pudritz R. E., 1992, ApJ 394, 117

Perley R. A., Dreher J. W., Cowan J. J., 1984, ApJ Letters 285, L35

Potash R. I., Wardle J. F. C., 1980, ApJ 239, 42

Pounds K. A., Reeves J. N., 2009, MNRAS 397, 249

Proga D., Jiang Y.-F., Davis S. W., Stone J. M., Smith D., 2014, ApJ 780, 51

Proga D., Kallman T. R., 2004, ApJ 616, 688

Proga D., Kurosawa R., 2010, in L. Maraschi, G. Ghisellini, R. Della Ceca, F. Tavecchio (eds.), Accretion and Ejection in AGN: a Global View, Vol. 427 of *Astronomical Society of the Pacific Conference Series*, 41

Proga D., Stone J. M., Kallman T. R., 2000, ApJ 543, 686

Reeves J. N., O'Brien P. T., Ward M. J., 2003, ApJ Letters 593, L65

Reichard T. A., Richards G. T., Hall P. B., Schneider D. P., Vanden Berk D. E., Fan X., York D. G., Knapp G. R., Brinkmann J., 2003, AJ 126, 2594

Risaliti G., Elvis M., Nicastro F., 2002, ApJ 571, 234

Shakura N. I., Sunyaev R. A., 1973, A&A 24, 337

Shlosman I., Vitello P., 1993, ApJ 409, 372

Shlosman I., Vitello P. A., Shaviv G., 1985, ApJ 294, 96

Silk J., Rees M. J., 1998, A&A 331, L1

Sim S. A., Long K. S., Miller L., Turner T. J., 2008, MNRAS 388, 611

Simon L. E., Hamann F., 2010, MNRAS 409, 269

Sutherland R. S., 1998, MNRAS 300, 321

Tombesi F., Cappi M., Reeves J. N., Palumbo G. G. C., Yaqoob T., Braito V., Dadina M., 2010, A&A 521, A57

Turner T. J., Miller L., 2009, AAPR 17, 47

Verner D. A., Ferland G. J., Korista K. T., Yakovlev D. G., 1996, ApJ 465, 487

Weymann R. J., Morris S. L., Foltz C. B., Hewett P. C., 1991, ApJ 373, 23

Weymann R. J., Scott J. S., Schiano A. V. R., Christiansen W. A., 1982, ApJ 262, 497

Zhang S. N., Cui W., Chen W., 1997, ApJ Letters 482, L155